Received: 10 September 2022 | Revised: 24 May 2023 | Accepted: 25 May 2023

DOI: 10.1002/jwmg.22459

THE JOURNAL OF WILDLIFE MANAGEMENT | THE WILDLIFE SOCIETY

FEATURED ARTICLE

A spatial, closed integrated population model to estimate wildlife population size and structure

Thomas Connor[1] | Emilio Tripp[2] | B. J. Saxon[2] | Jessica Camarena[2] | Jesse A. Goodwin[2] | William T. Bean[3] | Dan Sarna[1] | Justin Brashares[1]

[1]Department of Environmental Science, Policy, and Management, University of California, Berkeley, Mulford Hall, 130 Hilgard Way, Berkeley, CA 94720, USA

[2]Wildlife Division, Karuk Department of Natural Resources, 39051 CA-96, Orleans, CA 95556, USA

[3]Department of Biology, California Polytechnic State University, 1 Grand Avenue, San Luis Obispo, CA 93407, USA

Correspondence
Thomas Connor, Department of Environmental Science, Policy, and Management, University of California, Berkeley, Mulford Hall, 130 Hilgard Way, Berkeley, CA 94720, USA.
Email: connort@berkeley.edu

Funding information
California Department of Fish and Wildlife, Grant/Award Number: 6085-01

Abstract

Noninvasive data collection methods are increasingly used to monitor endangered, cryptic, or otherwise difficult to observe wildlife populations. Spatial capture-recapture and count-based statistical methods are often used to model these data to derive population estimates, each with their own advantages. The goal of our study was to integrate these 2 data sources and model structures to maximize the use of single-season surveys in which capture-recapture and count-based data are collected. We formulated a Bayesian spatial, closed integrated population model (cIPM) that leverages scat DNA-based spatial capture-recapture and camera-based spatial count sub-models to derive sex and age class-specific population estimates. Our cIPM has the advantage of sharing the spatial scaling (σ) parameter directly between sub-models and drawing proposed individuals from the same data-augmented superpopulation for each sub-model. This allows for separate estimation of sex and age-class groups simultaneously without any assumptions of population structure or conversions between model output types. We applied our cIPM to a wild population of Roosevelt elk (*Cervus canadensis roosevelti*, Karuk: íshyuux) during winter 2018–2019 in their winter range within Karuk Ancestral Territory in northern California, USA. We also conducted a simulation study to test

our cIPM on a known population consisting of 2 age classes and 2 sexes. The cIPM was able to estimate most population, detection, and σ parameters with good accuracy, including population size. The assignment of sex and age was biased, however, resulting in fewer juvenile males, more juvenile females, and more adult males. Our cIPM applied to the data estimated approximately 310 (95% CI = 235–411) female adults, 90 (95% CI = 57–134) male adults, 75 (95% CI = 43–149) female calves, and 23 (95% CI = 12–47) male calves. These estimates were different from those that would have been made had we relied on common assumptions such as equal calf sex ratios, though this ratio was likely biased towards females based on our simulation results. Our methods are widely applicable and maximize the amount of information available to managers and researchers from any single-season survey in which separate data sources capturing sex and age-class information are obtained.

KEYWORDS

ecological modeling, elk, integrated population model, population ecology, spatial capture-recapture, wildlife management

The estimation of wildlife population size is a core facet to ecological research, management, and conservation endeavors worldwide (Leopold 1933, Buckland et al. 2000). For species that occur in forested and rugged environments or are relatively cryptic, direct observation and counts are often unfeasible (Balme et al. 2009). In these cases, the use of noninvasive sampling methodologies can alleviate issues with animal detectability. For example, scat or hair-based DNA tagging can capture and recapture individuals across time and space without an observer ever directly seeing them. Similarly, methods using motion-sensitive cameras can detect species presence, derive counts, and potentially differentiate individuals that have unique visual patterning such as spots or stripes (Royle et al. 2009, Linkie et al. 2013). To make use of these noninvasive data sources, a variety of statistical methods have been adapted and developed to estimate population sizes based on individual capture-recapture data, animal count data, and animal presence-absence data (Efford and Fewster 2013, Gilbert et al. 2020).

For species that are visually identifiable by sex (via camera images) or for which a sex-specific primer has been developed and analyzed (for noninvasive genetics), sex-specific model parameters may be estimated (Gardner et al. 2010). At the very least, the estimation of population sex ratios allows for a more detailed understanding of the study population's ecology, potential recruitment rates, and viability (Bender 2006, Lounsberry et al. 2015). Information on sex also allows for the specification of detection probability, space use (for spatial models), and other parameters of interest that vary by sex, potentially enhancing model fit. Another important aspect of all populations is age structure, especially for harvested species because managers must obtain separate estimates of adult and juvenile population sizes to sustainably set harvest quotas (Bender 2006, Furnas et al. 2018). Noninvasive genetic capture-recapture, widely considered the gold standard for estimating population sizes in settings where wildlife is difficult to observe, is generally unable to differentiate between age classes because of the similarity of scats and hair by age class.

Although integrating data from different sources is increasingly used to improve model precision (Gopalaswamy et al. 2012, Clare et al. 2017, Ruprecht et al. 2021), very little work has been done to take advantage of model integration

to estimate sex and age class-specific abundance in a closed population setting. A notable example, however, is the integration of scat-based genetic spatial capture-recapture (SCR) data with camera-based site-count data in a closed integrated population model (cIPM) to derive separate estimates of adult female, adult male, and juvenile deer population sizes (Furnas et al. 2018). While the integrated model of Furnas et al. (2018) represents substantial progress over single or even sex-specific population estimates of managed wildlife populations, the authors relied on fundamentally different population sub-models whose outputs had to be converted (non-spatial site abundance to density) to be comparable and relied on the assumption of equal juvenile sex ratios to derive their estimates (Furnas et al. 2018).

We advanced the ideas of Furnas et al. (2018) by deriving a DNA- and camera-based cIPM in a Bayesian framework that takes further advantages of model integration to derive parameter estimates (separate adult female, adult male, juvenile female, and juvenile male population estimates) not identifiable by separate models alone (Plard et al. 2019). Specifically, we formulated our cIPM with 2 main objectives: 1) leverage the DNA- and camera-based sub-models to derive sex and age ratios directly estimated as probability distributions on the overall population and 2) make each sub-model explicitly spatial so that spatial information could be shared across sub-models without the need to estimate effective sampling areas to convert between model outputs.

STUDY AREA

We fit our cIPM to data collected on a Roosevelt elk (*Cervus canadensis roosevelti*; Karuk: íshyuux) population along the Klamath River in Karuk Ancestral Territory in northwestern California, USA. All our sampling took place in an approximately 528-km^2 area consisting of private and national forest land between November 2018 and May 2019, effectively capturing the overwintering habitat of a population of Roosevelt elk in the region. The drier summer season lasts from approximately June through October, when elk in our study population spend time at higher elevations in the Marble Mountains. Though historically much of the forests in this area were logged, there is currently minimal logging activity but increasing prescribed burning to manage for culturally important natural resources and reduce fuel loads. The rugged mountains and river valleys in this coastal range host a floristically diverse community dominated by a coniferous overstory consisting of Douglas-fir (*Pseudotsuga menziesii* var. *menziesii*), incense cedar (*Calocedrus decurrens*), sugar pine (*Pinus lambertiana*), Jeffrey pine (*P. jeffreyi*), and white fir (*Abies concolor*; Taylor and Skinner 2003). Other common large mammals (Karuk: mâakamkuuk) besides elk in the area include black bear (*Ursus americanus*; Karuk: vírusur), black-tailed deer (*Odocoileus hemionus*; Karuk: púufich), and mountain lion (*Puma concolor*; Karuk: yupthúkirar). The climate is Mediterranean with temperatures ranging from lows of around 0°C in December and January to highs of >30°C in August (Sawyer 2006). The Karuk Tribe have inhabited the area for thousands of years, and historically used elk for sustenance, art, and religious ceremony. Upon the arrival of Euro-Americans to Karuk Ancestral Territory in the 1800s, however, elk were extirpated, and the Karuk people were killed, displaced, and prevented from performing traditional fire-based habitat management practices for ungulates (Norgaard 2014).

Elk were reintroduced to the area over several translocation events starting in 1985 (Allison et al. 2007). By 1992, 232 had been reintroduced to the Klamath National Forest and Marble Mountain Wilderness areas by the National Forest Service and the California Department of Fish and Wildlife (Allison et al. 2007). Most elk herds in the area appear to undergo seasonal migration behavior, staying at relatively low elevations in the Klamath River Valley and ascending to high elevations to graze in the adjacent Marble Mountains in summer. Generally, Roosevelt elk exist in herds of adult females and juveniles, while adult males are more transient and frequently form smaller groups of their own outside of the mating season, depending on population sizes (Weckerly 2020). While both females and males may disperse from their natal herds and range as they mature, this behavior is heavily biased towards males (Edge et al. 1986). Rough population estimates in recent years suggest that the reintroduction efforts have been successful and that there are up to 3,000 Roosevelt elk across the wider region (California Department of Fisheries and Wildlife [CDFW] 2018).

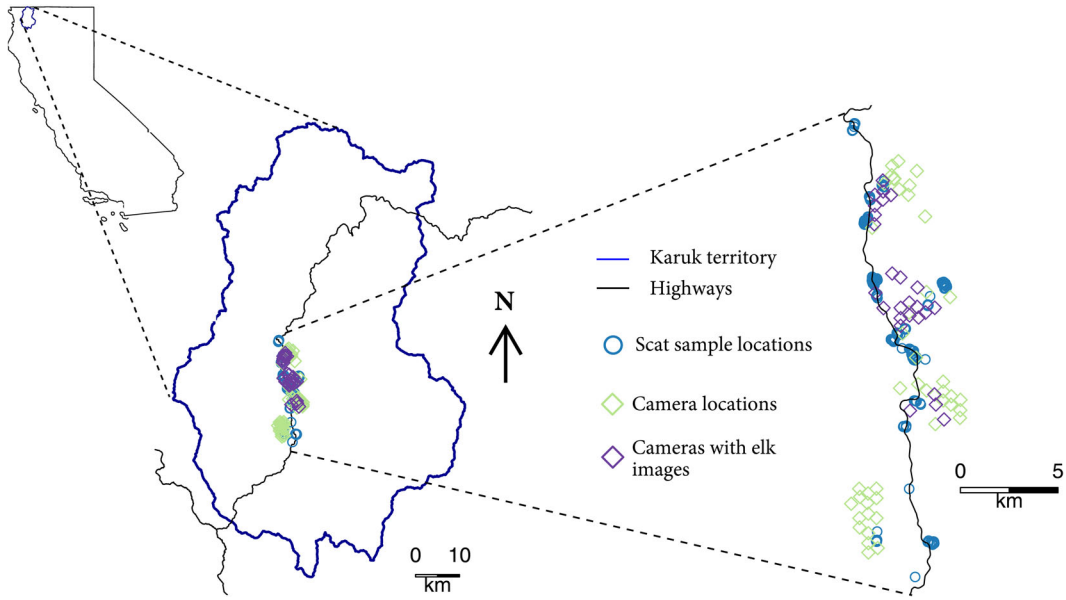

FIGURE 1 The study system, consisting of a core area of the Karuk Ancestral Territory inset on the state of California, USA, during winter of 2018–2019. All swabbed Roosevelt elk scat locations, motion-sensitive camera locations, and cameras with elk capture locations used to fit our Bayesian closed, integrated population model are presented.

METHODS

Scat collection

Our noninvasive scat DNA surveys were focused on elk winter range around the Klamath River in winter of 2018–2019. We collected scat systematically between December 2018 and April 2019 in an area-search approach at 13 focal sites throughout this area and visited each site between 1 and 3 times with revisits separated by at least 2 weeks (Figure 1). These area searches were informed by local Karuk traditional ecological knowledge (TEK) of elk space and habitat use throughout the area to maximize detectability while maintaining enough spatial extent to produce the recaptures across space for the SCR model. To facilitate SCR modeling in a Bayesian framework, we converted the area-search sampling effort to a virtual trapping grid with traps evenly spaced at 250 m using the discretize function in the secr R package (Efford 2019, R Core Team 2019). In this conversion, we assigned individuals identified through scat in the area search as caught in the nearest virtual trap <125 m distant. We used 250-m spacing of our virtual traps to balance spatial accuracy in capturing the actual scat locations and computational efficiency in reducing the number of traps to iterate through in the Bayesian model. We swabbed scat with a sterile cotton swab, which we then placed in test tubes containing Longmire buffer for storage and later DNA extraction and analysis. We used 8 microsatellite loci targeted with primers developed for tule elk (*Cervus canadensis nannodes*) for individual identification and a sex-specific marker (Sacks et al. 2016). To account for the potential of false alleles and allelic dropouts due to low-quality DNA, we repeated the genetic analysis of each sample twice and used the R package allelematch to assign individuals based on probabilities of allele mismatches (Galpern et al. 2012). For a full description of the genetics methods that we used, see Bach et al. (2022).

Camera grids

We established 4 hexagonal grid camera arrays across our study area in which we placed 15 cameras at the centers of the hexagons approximately 500 m apart (Figure 1). These 4 grids corresponded to focal areas of the Western Klamath Restoration Partnership's Somes Bar Integrated Project Area and were designed to monitor wildlife responses to forest management actions (Berger and Colegrove 2018). We maximized the likelihood of capturing wildlife by placing the cameras at approximately shoulder-height and directing the viewshed along game trails or areas with good visibility. We used Bushnell TrophyCam HD Aggressor cameras (Bushnell, Overland Park, KS, USA) set to take 2 photos at the detection of any movement under the low sensitivity setting with a medium shutter speed and a sleep time of 3 seconds between photo bursts. To match the temporal scope of the scat sampling efforts and to sample the population across winter, we ran the cameras from the end of November 2018 to the end of March 2019. We visited the cameras every 2 months to make sure they were operational and to collect and replace the memory cards.

We separated images of elk female adults, male adults, and calves into separate folders by looking for identifying traits including antlers and size. We then used the R package camtrapR to derive separate record tables for each (Niedballa et al. 2016). We defined single occasions as individual weeks of our study period and derived weekly counts of each class of elk by counting the maximum number of individuals in a single image over a 24-hour period and then summing those 7 24-hour counts. We did this to avoid either over-counting individuals that remained in front of a motion-sensitive camera for extended periods of time or under-counting individuals that occurred in the same image by defining that image as a single detected individual.

Closed integrated population model

Our Bayesian cIPM integrated scat-based SCR and camera-based unmarked SCR (uSCR, or spatial count) sub-models by directly linking their likelihoods to the same realized population drawn from a data-augmented superpopulation (Royle and Dorazio 2012). This data-augmentation approach draws actual members of the population from an unrealistically large superpopulation (M) through a probability of inclusion parameter (ψ). We set M = 1,000 so that it would not affect the realized population size estimates in the posterior distribution. The SCR and uSCR models follow the same general formulation in that they estimate the density of animal activity centers (s; tracked explicitly from the data in SCR and from a latent parameter in uSCR) across the study area. In SCR models, the probability of detecting an individual i at a trap j ($p_{i,j}$) is a function of a baseline detection probability ($p0$) and a spatial scaling parameter (σ) that describes the decline in the probability of detecting an individual as the Euclidean distance (d) between that individual's activity center (s_i) and the trap (j_i) increases (Efford and Fewster 2013):

$$p_{i,j} = p0 \times \exp\left(\frac{-d_{si,j}^2}{2\sigma^2}\right).$$

We then modeled the number of times an individual i was detected at a trap j as a Poisson random variable (Royle and Young 2008, Royle et al. 2009):

$$y_{i,j} \sim \text{Poisson}(p_{i,j} \times z_i),$$

where z_i takes the value of 1 if the individual was drawn from the data-augmented superpopulation M and 0 if it was not, dictated by Bernoulli draws with probability of inclusion, ψ:

$$z_i \sim \text{Bernoulli}(\psi)$$

Ultimately, the total population size is derived by summing the number of $z = 1$ individuals that are estimated to have activity centers within the study area:

$$N = \sum_{i=1}^{M} z_i.$$

In uSCR models, probability of detection and spatial scaling parameters also apply in the same way, but as opposed to modeling counts of an individual's detections, the count of the number of individuals detected at a trap (j) are modeled instead (Chandler and Royle 2013):

$$\Lambda_j = \lambda 0 \times \exp\left(\frac{-d_{si,j}^2}{2\sigma^2}\right),$$

where λ0 is a probability of detection parameter specific to the motion-sensitive camera data collection process, but the spatial scaling parameter (σ) is directly shared with the SCR sub-model. The trap-specific counts are then modeled as a Poisson random variable:

$$n_j \sim \text{Poisson}(\Lambda_j).$$

We integrated the genetics-based SCR and camera-based uSCR sub-models defined above in a Bayesian framework with the following joint posterior distribution:

$$[z_i, \psi, \sigma, s_i, \text{p0}, \lambda 0 | y_{i,j}, n_j, x.\ genetics_j, x.\ camera_j]$$

$$\propto \text{Genetic SCR: } \prod_{i=1}^{M} \prod_{j=1}^{J} \text{Poisson}(y_{i,j} | f(\text{p0}, z_i, \psi, \sigma, s_i, x.\ genetics_j))$$

$$\times \text{Camera uSCR: } \prod_{i=1}^{M} \prod_{j=1}^{J} \text{Poisson}(n_j | f(\lambda 0, z_i, \psi, \sigma, s_i, x.\ camera_j))$$

where x corresponds to the spatial coordinates of trap j.

Because both SCR and uSCR estimate the activity centers (s) of individuals in the population, those activity centers could be directly integrated across sub-models. Because our scat sampling and camera data collection efforts did not cover exactly the same area (Figure 1), however, we proposed separate activity centers for the same individuals for each sub-model but shared the spatial scaling (σ) parameter between the sub-models (Ruprecht et al. 2021). This assumes that although the scat and camera arrays were covering slightly different areas, they were sampling the same individuals in the same population. Given the relatively large winter home ranges of elk in the area (~20 km^2; Connor et al. 2022) compared to the relatively small spatial mismatch of the trapping arrays (<3 km; Figure 1), we think this assumption that we sampled the same individuals through both data collection methods holds well.

We included a probability of being a male and a probability of being an adult parameter as draws from a Bernoulli distribution. The SCR sub-model informed the sex probability of each individual through the amplification of a sex-specific loci in the scat DNA data. The uSCR sub-models provided the sex of adult individuals and the age class probability of each individual based on identification from the camera data. Directly integrating the sub-models by sampling the same data-augmented superpopulation and harnessing their separate power to estimate sex and age class in this way allowed us to separately estimate the population sizes of female adults, male adults, female calves, and male calves. To account for differences in space use and the probability of detecting male adults versus female adults and calves, we estimated separate spatial scaling (σ) and probability of detection parameters for adult males and adult females and calves. We grouped females and

calves for these parameters because we expected their space use and probability of detection to be similar (calves traveling with their maternal herd). We specified these separate σ values in the model by creating an indicator for each individual in the Markov chain Monte Carlo (MCMC) iterations that specified if they were either an adult male or an adult female or calf, and this indicator then pointed to which of the 2 σ values to estimate and use for that individual.

We set uninformative prior distributions on ψ (probability of inclusion), sex probability, and age probability using beta distributions with both shape parameters = 1. We set a weakly informative prior on σ using a uniform distribution bounded by 0 and 5,000 m, capturing possible corresponding home range sizes from 0 to 471 km^2. We used weakly informative priors on both baseline detection probabilities (scat and camera) defined as the logit transformation of a draw from a uniform distribution bounded by −6 and 1. We conducted all analyses using the Nimble language in R (de Valpine et al. 2017, R Core Team 2019). We ran MCMC chains for 60,000 iterations with default random walk settings for all parameters, and a burn-in of 20,000 for chains to converge. We assessed chain convergence using the Monte Carlo standard error as a percentage of the posterior standard deviation (MCEpc) diagnostic, and a visual inspection of the MCMC trace plots.

Simulation study

To test the performance of our cIPM under known conditions, we simulated a sex- and age-structured population followed by both SCR and count sampling of that population. We used the sim.capthist function of the secr R package (Efford 2019) to facilitate this simulation for each of 4 sex-age classes (adult females, adult males, juvenile females, juvenile males) in 3 steps: 1) simulate animal activity centers across an area of 136,900 m^2, 2) simulate capture-recapture sampling of those animals across a 15 by 15 square grid of 100 artificial traps spaced 20 m apart, and 3) derive counts for adult females, adult males, and juveniles (grouped) at each trap by summing the number of individual captures at each trap. We set the $p0$ and σ parameters, which along with simulated density determines the capture history at each trap, as follows: a $p0$ of 0.3 for all sex and age classes, and a σ value of 15 m for adult females and juveniles and 20 m for adult males. We were especially interested in the ability of our model to estimate the sex of individuals when the sex ratios differed between age classes, so we simulated population densities so that there were 3 adult females (15/ha) per adult male (5/ha) but a 1 to 1 (even) sex ratio in juveniles (3.75/ha for each sex). We used the same specifications and priors in fitting the cIPM as described in our empirical study but ran only 13,000 MCMC iterations with 3,000 used as a burn-in.

RESULTS

We located 748 elk scats across the 10 sampling sites; 289 were successfully genotyped. From these 289 samples, we identified 114 unique individuals captured between 1 and 13 times each, resulting in an average capture rate of 2.54 captures/individual. Of the 61 deployed motion-sensitive cameras, 21 captured images of elk on at least one occasion. Specifically, 12 cameras captured female adults with occasion-level counts ranging from 1 to 31, 10 cameras captured male adults with occasion-level counts ranging from 1 to 4, and 8 cameras captured calves with occasion-level counts ranging from 1 to 12.

Our Bayesian cIPM showed good convergence, with low MCEpc values and adequate mixing in the trace plots (Figure S2, available in Supporting Information). The model estimated 523 elk (mean of the posterior) across our study area (95% CI = 422–639; Table 1; Figure 2), corresponding to a density of about 0.92 elk/km^2. The estimated sex ratio was skewed towards female (0.78:0.22), and the estimated age class ratio was skewed towards adults (0.79:0.21; Table 1). The female-biased sex ratio was in both adult and calf age classes but was larger in the adult age class. The estimated spatial scaling (σ) parameter was 1.02 km (95% CI = 0.91–1.12) for female adults and

TABLE 1 Parameter estimates from the posterior distributions of a Bayesian closed, integrated population model fit to data from Roosevelt elk in Karuk Ancestral Territory, California, USA, during winter of 2018–2019.

Parameter[a]	$\bar{x}$	SD	Lower credible interval (2.5% quantile)	Upper credible interval (97.5% quantile)
Total population size	523	55.77	422	639
Female adults	310	45.27	235	411
Male adults	90	19.94	57	134
Female calves	89	27.55	43	149
Male calves	27	9.79	11	49
Adult male $p0$ scat	0.19	0.05	0.09	0.30
Female adult and calf $p0$ scat	0.56	0.07	0.44	0.70
Male adult λ0 cameras	0.05	0.02	0.02	0.10
Female adult and calf λ0 cameras	0.68	0.05	0.56	0.72
Male adult σ (km)	2.32	0.37	1.93	3.43
Female adult and calf σ (km)	1.02	0.05	0.91	1.12
Sex ratio (probability male)	0.22	0.04	0.14	0.32
Age class ratio (probability adult)	0.79	0.06	0.64	0.89

[a]$p0$ = probability of detection via scat, λ0 = probability of detection via camera, σ = space use parameter describing decline in probability of detection over increasing distance.

2.52 km (95% CI = 1.93–3.43) for adult males, corresponding to an average circular home range (using the conversion home range radius = 2.45 × σ) of approximately 19.62 km^2 and 119.75 km^2, respectively. There was a lower probability of detecting adult males by scat DNA (0.19, 95% CI = 0.09–0.30) and cameras (0.05, 95% CI = 0.02–0.10) compared to adult females and calves (scat DNA: $p0$ = 0.56, 95% CI = 0.44–0.70; cameras: λ0 = 0.68, 95% CI = 0.56–0.72; Table 1).

The posterior distributions of most of the parameters in the cIPM fit to our simulated population closely matched the parameters used to simulate the population, but there was some error in correctly assigning sex and age classes (Figure S1; Figure 3). While the overall population size was estimated accurately (within 1.5% of the simulated values), adult males and juvenile females were overestimated, whereas juvenile males were underestimated, resulting in a skewed juvenile sex ratio with over double the estimated females compared to males (Figure 3; Table S1, available in Supporting Information). Most of the $p0$ and σ parameters were estimated accurately, with only the probability of detection for adult males in the uSCR count process estimated at more than 10% off the simulated value (estimated at 0.26 and simulated at 0.3; Table S1).

DISCUSSION

Our Bayesian cIPM has several advantages over existing methods for the monitoring and management of ungulate populations. First, directly integrating scat DNA-based and camera-based sub-models through the use of SCR and uSCR methods allowed for the joint estimation of the σ parameter. Because σ is notoriously difficult to compare across data sources and spatial modeling methods, directly linking it in a cIPM increases the relevancy of spatial sub-models to each other and helps identify it in sub-models relying on data with inherently little space-use

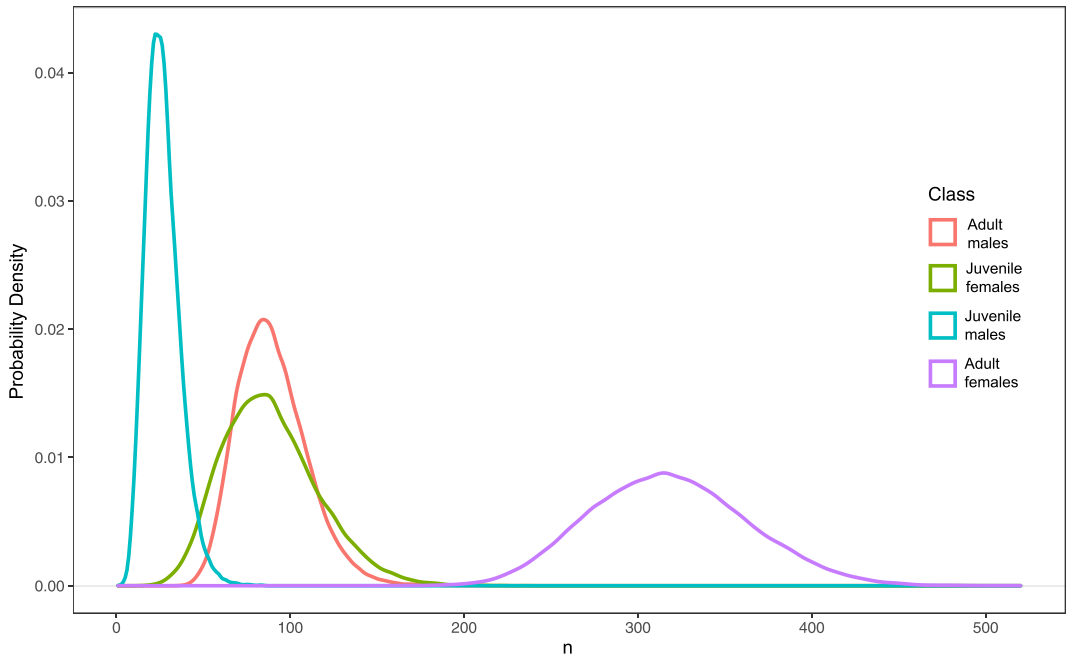

FIGURE 2 Posterior distributions of the population size estimates from the Bayesian closed, integrated population model fit to empirical data collected on Roosevelt elk in Karuk Ancestral Territory, California, USA, during winter of 2018–2019 by sex and age class.

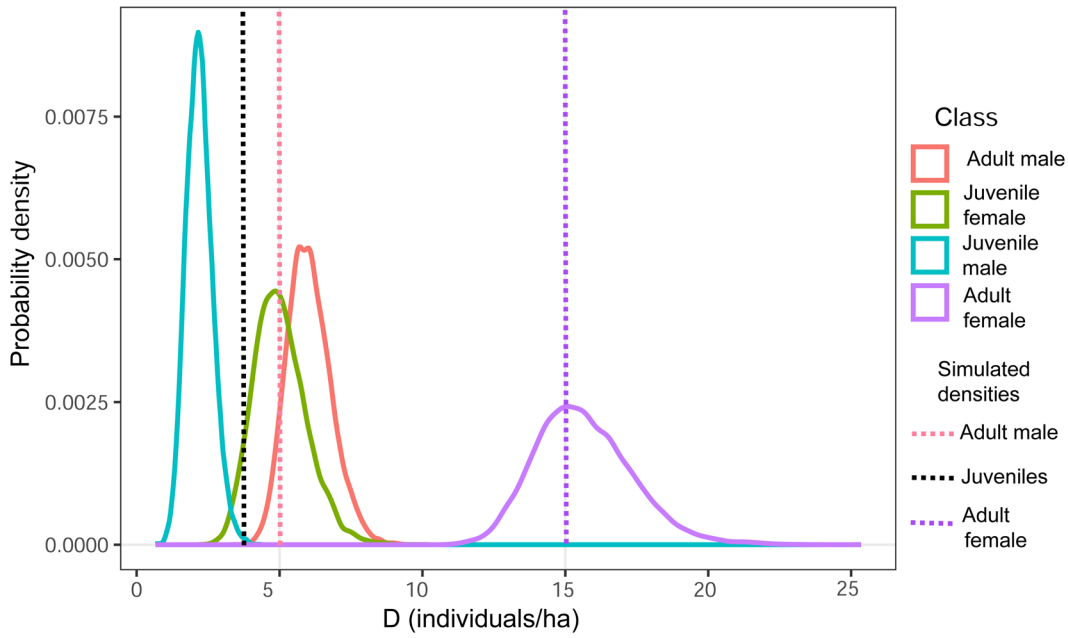

FIGURE 3 Posterior distributions of the population density (D) estimates from the Bayesian closed, integrated population model fit to simulated data by sex and age class. Vertical dotted lines represent the true population density of a simulated elk population.

information such as uSCR (Ramsey et al. 2015, Ruprecht et al. 2021). Further information on animal movement, such as global positioning system (GPS) collar telemetry data, could also be used to inform σ through a prior distribution (Furnas et al. 2018) or directly integrated in the IPM to help estimate σ (Ruprecht et al. 2021).

Additionally, the direct integration of our scat DNA-based SCR and camera-based uSCR models had the advantage of unlocking population estimates for sex and age classes unidentifiable by the sub-models alone (Riecke et al. 2019). For example, although camera-based uSCR models can produce separate estimates of female adults, male adults, and calves, the sex of calves generally cannot be determined through camera images (Macaulay et al. 2020). Conversely, although the age class of individuals is generally unknown through scat-based DNA, the sex of every individual can be identified (Sacks et al. 2016). By integrating both data sources and sub-models directly in an IPM, each sex and age class can be separately estimated. This is a potential advantage over previous closed-population IPMs that must assume equal sex ratios in juveniles (Furnas et al. 2020).

Although our estimated population size of 523 individuals is less than the approximately 3,000 individuals estimated throughout the region in past years, our study area was only 568 km^2, translating to an estimated density of 0.92 elk/km^2. If we extrapolate this finding to the area that falls within the approximate elk winter range in Karuk Ancestral Territory, the population for that area is estimated at an unrealistic >50,000. This extrapolated region likely includes large areas of poor elk habitat compared to our study area, and more sampling efforts across wider areas of Karuk Ancestral Territory and the Marble Mountain elk management zone are needed to get a fuller and more nuanced understanding of the Roosevelt elk populations that reside there. Because of the difficultly in conducting many traditional ungulate sampling methods in the rugged and forested terrain, robust population estimates have been difficult to derive in the region (CDFW 2018). In solving this issue through noninvasive sampling informed by local expertise, our study advances multiple goals in California's elk management plan, including developing robust methods for population estimation and increasing collaboration with California's Tribes (CDFW 2018).

Going beyond grouped population estimates and considering sex and age structure, our results indicate that assuming even sex ratios in juveniles in this population would be invalid, and that there are more female calves compared to male calves. Because the sex ratio for calves was nearly as female-skewed as that of adults is puzzling because we expected the sex ratio to be relatively more equal at younger ages before extensive dispersal behavior (Petersburg et al. 2000). Potential biological reasons for the skewed sex ratio in calves that we estimated include higher birth rates for female calves and lower male calf survival rates due to behavioral differences in calves by sex, or behavioral and physiological differences in mothers influencing calf survival by sex (Kohlmann 1999, Cunningham et al. 2009). Additionally, early dispersal events, a behavior likely biased towards the male calves, could result in more male calves leaving our study area entirely and facing higher mortality during dispersal (Smith and Anderson 2001).

Though there are potential biological reasons for the skewed juvenile sex ratio, our simulation study also suggests that our model has the tendency to falsely estimate skew in the juvenile sex ratio when the adult sex ratio is skewed (as is common in ungulate populations; Berger and Gompper 1999). While overall population density estimates were accurately estimated, the even juvenile sexes were generally estimated at around 40% fewer males and 34% more females than expected. The adult males were overestimated at a rate similar to which the juvenile males were underestimated, suggesting that correcting this biased male age class assignment in the model would largely solve the issue. Improving the σ estimation for adult males through the incorporation of GPS telemetry data could correct the issue (Furnas et al. 2020, Ruprecht et al. 2021). These results suggest a significant bias and the need to more accurately separate juvenile and adult sex ratios in future implementations of our cIPM. That said, separately estimating female and male calf population sizes in our empirical study using our cIPM likely produced results with about the same bias compared to assuming an even juvenile sex ratio, given the very large differences (~3 times the juvenile females compared to males) we found. If our empirical study had a bias of the same magnitude evident in our simulation study, the real probability of being male in the juvenile age class was approximately 0.37.

In addition to improving the separation of juvenile and adult sex ratios, perhaps through the integration of other data sources like GPS telemetry, there is room for further improvements and advancements. Modeling of animal activity centers as a function of environmental covariates on the landscape would provide ecological inference on the factors influencing population density and allow for the projection of the cIPM to estimate population sizes across wider areas (Furnas et al. 2018, Connor et al. 2022). Also, the use of multiple years of SCR and spatial count data would allow for the specification of a novel spatial open-population IPM that estimates both population size and demographic rates by sex and age class (Plard et al. 2019).

MANAGEMENT IMPLICATIONS

Wildlife managers and conservationists must make decisions based on the best available information and often considering diverse perspectives. We posit that our Bayesian cIPM, as presented here, leverages commonly collected noninvasive genetics and motion-sensitive camera datasets to maximize the amount of biological information that can be derived in a single-season survey. For harvested populations in particular, our separation of population estimates by sex and age class provides critical information that can help set harvest regulations based on population structure. For example, if few juvenile females are detected in a given year, adult female harvest could be reduced to account for the smaller number of incoming females to that age class in subsequent years and subsequent lower reproductive potential of the population. The application of Karuk TEK was an important piece of our study that increased the feasibility of fitting effective SCR models through increased detectability of elk. Such local knowledge is invaluable for effective conservation and management through enhanced data collection as described here, but also the interpretation and application of findings derived from wildlife surveys in a given study system. In conclusion, the methods we developed can be applied to any population for which simultaneous individual capture-recapture and spatial count data is collected across the study area of interest, and their careful application will improve the monitoring and management of difficult-to-observe wildlife populations.

CONFLICT OF INTEREST STATEMENT

The authors declare no conflicts of interest.

ETHICS STATEMENT

This study adhered to proper animal welfare guidelines as outlined by the Karuk Tribe, the University of California, and American Society of Mammologists (Sikes 2016), and followed the study plan approved in the California Department of Fish and Wildlife grant P1780108. Because this research did not involve the direct handling of wildlife and only non-invasive data (scat and motion-sensitive camera images) was collected, this study did not require an Animal Use Protocol from the University of California, Berkeley.

DATA AVAILABILITY STATEMENT

R code to run the cIPM and simulation is published on Figshare at this link: https://figshare.com/s/6ba611eb699fc232bce6. Elk data will be available by request and approval of the Karuk Tribe Department of Natural Resources.

ORCID

Thomas Connor http://orcid.org/0000-0002-7630-5156

REFERENCES

Allison, B. L., M. Creasy, M. Ford, A. Hacking, R. Schaefer, J. West, and Q. Youngblood. 2007. Elk management strategy Klamath National Forest. U.S. Forest Service Report, Klamath National Forest, Orleans, California, USA.

Bach, B. H., A. B. Quigley, K. M. Gaynor, A. McInturff, K. L. Charles, J. Dorcy, and J. S. Brashares. 2022. Identifying individual ungulates from fecal DNA: a comparison of field collection methods to maximize efficiency, ease, and success. Mammalian Biology 102:863–874.

Balme, G. A., L. T. B. Hunter, and R. Slotow. 2009. Evaluating methods for counting cryptic carnivores. Journal of Wildlife Management 73:433–441.

Bender, L. C. 2006. Uses of herd composition and age ratios in ungulate management. Wildlife Society Bulletin 34: 1225–1230.

Berger, E. A., and N. C. Colegrove 2018. Somes Bar Integrated Fire Management Project: environmental assessment. U.S. Forest Service, Siskiyou County, Orleans, California, USA.

Berger, J., and M. E. Gompper. 1999. Sex ratios in extant ungulates: products of contemporary predation or past life histories? Journal of Mammalogy 80:1084–1113.

Buckland, S. T., I. B. J. Goudie, and D. L. Borchers. 2000. Wildlife population assessment: past developments and future directions. Biometrics 56:1–12.

California Department of Fisheries and Wildlife [CDFW]. 2018. Elk conservation and management plan. California Department of Fisheries and Wildlife, Sacramento, USA.

Chandler, R. B., and J. A. Royle. 2013. Spatially explicit models for inference about density in unmarked or partially marked populations. Annals of Applied Statistics 7:936–954.

Clare, J., S. T. McKinney, J. E. DePue, and C. S. Loftin. 2017. Pairing field methods to improve inference in wildlife surveys while accommodating detection covariance. Ecological Applications 27:2031–2047.

Connor, T., W. Division, E. Tripp, W. T. Bean, B. J. Saxon, J. Camarena, A. Donahue, D. Sarna-Wojcicki, L. Macaulay, W. Tripp, and J. Brashares. 2022. Estimating wildlife density as a function of environmental heterogeneity using unmarked data. Remote Sensing 14:1087.

Cunningham, J. A., K. L. Hamlin, and T. O. Lemke. 2009. Fetal sex ratios in southwestern Montana elk. Journal of Wildlife Management 73:639–646.

de Valpine, P., D. Turek, C. J. Paciorek, C. Anderson-Bergman, D. T. Lang, and R. Bodik. 2017. Programming with models: writing statistical algorithms for general model structures with NIMBLE. Journal of Computational and Graphical Statistics 26:403–413.

Edge, W. D., C. L. Marcum, S. L. Olson, and J. F. Lehmkuhl. 1986. Nonmigratory cow elk herd ranges as management units. Journal of Wildlife Management 50:660–663.

Efford, M. 2019. secr: spatially explicit capture-recapture in R. Version 4.5.10. https://cran.r-project.org/web/packages/secr/index.html

Efford, M. G., and R. M. Fewster. 2013. Estimating population size by spatially explicit capture-recapture. Oikos 122: 918–928.

Furnas, B. J., R. H. Landers, S. Hill, S. S. Itoga, and B. N. Sacks. 2018. Integrated modeling to estimate population size and composition of mule deer. Journal of Wildlife Management 82:1429–1441.

Furnas, B. J., R. H. Landers, R. G. Paiste, and B. N. Sacks. 2020. Overabundance of black-tailed deer in urbanized coastal California. Journal of Wildlife Management 84:979–988.

Galpern, P., M. Manseau, P. Hettinga, K. Smith, and P. Wilson. 2012. Allelematch: an R package for identifying unique multilocus genotypes where genotyping error and missing data may be present. Molecular Ecology Resources 12: 771–778.

Gardner, B., J. A. Royle, M. T. Wegan, R. E. Rainbolt, and P. D. Curtis. 2010. Estimating black bear density using DNA data from hair snares. Journal of Wildlife Management 74:318–325.

Gilbert, N. A., J. D. Clare, J. L. Stenglein, and B. Zuckerberg. 2020. Abundance estimation methods for unmarked animals with camera traps. Conservation Biology 35:88–100.

Gopalaswamy, A. M., J. A. Royle, M. Delampady, J. D. Nichols, K. U. Karanth, and D. W. Macdonald. 2012. Density estimation in tiger populations: combining information for strong inference. Ecology 93:1741–1751.

Kohlmann, S. G. 1999. Adaptive fetal sex allocation in elk: evidence and implications. Journal of Wildlife Management 63: 1109–1117.

Leopold, A. 1933. Game management. University of Wisconsin Press, Madison, USA.

Linkie, M., G. Guillera-Arroita, J. Smith, A. Ario, G. Bertagnolio, F. Cheong, G. R. Clements, Y. Dinata, S. Duangchantrasiri, G. Fredriksson, et al. 2013. Cryptic mammals caught on camera: assessing the utility of range wide camera trap data for conserving the endangered Asian tapir. Biological Conservation 162:107–115.

Lounsberry, Z. T., T. D. Forrester, M. T. Olegario, J. L. Brazeal, H. U. Wittmer, and B. N. Sacks. 2015. Estimating sex-specific abundance in fawning areas of a high-density Columbian black-tailed deer population using fecal DNA. Journal of Wildlife Management 79:39–49.

Macaulay, L. T., Sollmann, R., & Barrett, R. H. (2020). Estimating deer populations using camera traps and natural marks. The Journal of Wildlife Management, 84:301–310.

Niedballa, J., R. Sollmann, A. Courtiol, and A. Wilting. 2016. camtrapR: an R package for efficient camera trap data management. Methods in Ecology and Evolution 7:1457–1462.
Norgaard, K. 2014. The politics of fire and the social impacts of fire exclusion on the Klamath. Humboldt Journal of Social Relations 36:77–101.
Petersburg, M. L., A. W. Alldredge, and W. J. de Vergie. 2000. Emigration and survival of 2-year-old male elk in northwestern Colorado. Wildlife Society Bulletin 28:708–716.
Plard, F., R. Fay, M. Kery, A. Cohas, and M. Schaub. 2019. Integrated population models: powerful methods to embed individual processes in population dynamics models. Ecology 100:e02715.
R Core Team. 2019. R Foundation for Statistical Computing, Vienna, Austria.
Ramsey, D. S. L., P. A. Caley, and A. Robley. 2015. Estimating population density from presence-absence data using a spatially explicit model. Journal of Wildlife Management 79:491–499.
Riecke, T. V., P. J. Williams, T. L. Behnke, D. Gibson, A. G. Leach, B. S. Sedinger, P. A. Street, and J. S. Sedinger. 2019. Integrated population models: model assumptions and inference. Methods in Ecology and Evolution 10:1072–1082.
Royle, J. A., and R. M. Dorazio. 2012. Parameter-expanded data augmentation for Bayesian analysis of capture-recapture models. Journal of Ornithology 152:S521–S537.
Royle, J. A., K. U. Karanth, A. M. Gopalaswamy, and N. S. Kumar. 2009. Bayesian inference in camera trapping studies for a class of spatial capture-recapture models. Ecology 90:3233–3244.
Royle, J. A., and K. V. Young. 2008. A hierarchical model for spatial capture-recapture data. Ecology 89:2281–2289.
Ruprecht, J. S., C. E. Eriksson, T. D. Forrester, D. A. Clark, M. J. Wisdom, M. M. Rowland, B. K. Johnson, and T. Levi. 2021. Evaluating and integrating spatial capture-recapture models with data of variable individual identifiability. Ecological Applications 31:e02405.
Sacks, B. N., Z. T. Lounsberry, T. Kalani, E. P. Meredith, and C. Langner. 2016. Development and characterization of 15 polymorphic dinucleotide microsatellite markers for tule elk using HiSeq. 3000. Journal of Heredity 107:666–669.
Sawyer, J. O. 2006. Northwest California: a natural history. University of California Press, Berkeley, USA.
Sikes, R. S., and the Animal Care and Use Committee of the American Society of Mammalogists. 2016. Guidelines of the American Society of Mammalogists for the use of wild mammals in research and education. Journal of Mammalogy 97: 663–688.
Smith, B. L., and S. H. Anderson. 2001. Does dispersal help regulate the Jackson elk herd? Wildlife Society Bulletin 29: 331–341.
Taylor, A. H., and C. N. Skinner. 2003. Spatial patterns and controls on historical fire regimes and forest structure in the Klamath Mountains. Ecological Applications 13:704–719.
Weckerly, F. W. 2020. Frequency and density associated grouping patterns of male Roosevelt elk. Frontiers in Ecology and Evolution 8:204.

Associate Editor: Pietro Milanesi.

SUPPORTING INFORMATION

Additional supporting material may be found in the online version of this article at the publisher's website.

How to cite this article: Connor, T., E. Tripp, B. J. Saxon, J. Camarena, J. A. Goodwin, W. T. Bean, D. Sarna, and J. Brashares. 2023. A spatial, closed integrated population model to estimate wildlife population size and structure. Journal of Wildlife Management 87:e22459. https://doi.org/10.1002/jwmg.22459